The 4th European sCO2 Conference for Energy Systems
March 23-24, 2021, Online Conference

2021-sCO2.eu-132

NUMERICAL ANALYSIS OF A CENTRIFUGAL COMPRESSOR OPERATING WITH SUPERCRITICAL CO2

Renan Emre Karaefe*,
Pascal Post, Marwick Sembritzky, Andreas Schramm,
Francesca di Mare
Ruhr University Bochum
Faculty of Mechanical Engineering
Chair of Thermal Turbomachines and Aeroengines
44801 Bochum, Germany
Email: emre.karaefe@rub.de

Matthias Kunick
Zittau/Goerlitz University of Applied Sciences
Faculty of Mechanical Engineering
02763 Zittau, Germany

Uwe Gampe
Technische Universität Dresden
Faculty of Mechanical Science and Engineering
Chair of Thermal Power Machinery and Plants
01062 Dresden, Germany

ABSTRACT

This study investigates the performance of a centrifugal compressor stage operating with supercritical CO_2. The candidate geometry comprises a channel diffuser and is based on main dimensions of a test-loop compressor operated by Sandia National Laboratories. A non-dimensional performance curve is derived through three-dimensional RANS calculations performed with an in-house compressible CFD solver and is compared to experimental data as well as a meanline analysis that is conducted applying a single-zone modelling approach, including internal and external loss models. Within the CFD simulations, real gas thermophysical properties of carbon dioxide are assessed through an accurate and efficient tabulation procedure, the Spline-Based Table Look-Up Method (SBTL), which is optimised for the density-based solver architecture. The conducted RANS calculations show an ideal head rise of up to 41 % through the channel diffuser compared to an ideal head assessment considering the impeller. The applied meanline methodology provides good agreement with the impeller performance characteristics derived from RANS calculations over the entire investigated flow range. Except for flow coefficients exceeding values of $\phi \approx 0.043$, where an abrupt decrease of the ideal head recovery is identified in the CFD assessments, which is not resembled by the meanline diffuser model, also satisfactory agreement of the meanline stage performance characteristics with the CFD results is obtained. Hence, applicability of the corresponding meanline loss models for sCO_2 compressor analysis is indicated.

INTRODUCTION

Closed power cycles utilising supercritical carbon dioxide as the working fluid exhibit several advantages compared to conventional power cycles. These power systems are predominantly designed as Brayton cycles where the compression is conducted at thermodynamic states that are lying close to the vapour-liquid critical point of CO_2 and are therefore characterised by a high fluid density. Hence, compression work is reduced significantly. Furthermore, high fluid density enables compact component de-

*Address all correspondence to this author.

DOI: 10.17185/duepublico/73966

sign and ultimately paves the way for a small physical footprint of the overall plant. Supercritical power systems can also be coupled to a variety of heat sources, allowing for a broad range of applications.

Despite increased research efforts, there are still enduring challenges which need to be overcome until sCO_2 cycles can be commercialised. Key issues concern reliable process control, the design of compact and effective heat exchangers as well as the realisation of satisfactory turbomachinery performance characteristics. Predominantly, centrifugal compressors are applied in sCO_2 Brayton cycles and, in particular, the main compressor of a recompression layout is expected to be a radial configuration for a broad range of system scales due to its lower volume flow and wider range to facilitate variations in gas properties [8].

Design and analysis methods are sophisticated for centrifugal compressors operating with fluids obeying the ideal gas law. However, because of the scarcity of reference data, the validity of respective methods is still uncertain when these are applied to compressors operating with real fluids. In particular, fluid states near the critical point are characterised by highly non-linear and rapidly changing property behaviour. Adressing these issues, predictive CFD simulations, accounting for thermophysical real gas properties with a high degree of accuracy, allow for an insight into the dynamic development of flow field and are therefore an important tool to improve the aerothermal design and analysis of sCO_2 turbomachinery.

The majority of numerical studies of sCO_2 compressors in the literature refer to a main compressor geometry operated in a compression test-loop by Sandia National Laboratories (SNL). The compressor has undergone extensive testing and until today provides one of the very few cases for which experimental reference data as well as the respective compressor geometry is at least partially documented in the form of main dimensions. In one of the first studies related to the SNL compressor, Pecnik et al. [26] performed 3D RANS calculations of a main compressor impeller resembling the SNL main compressor design. A computed speed line indicated higher head generation compared to the experimental data used for validation purposes. Deviations were attributed to the simplified geometry not considering the vaned diffuser and the impeller clearance. Analysis of the flow field showed thermodynamic states of the flow domain lying within the vapour-liquid region. These were identified at the impeller blade tip suction side and the trailing edge, as a result of flow acceleration and the decrease of static conditions. In following studies of the research group, the complete stage geometry, comprising the vaned diffuser and tip clearance, was modeled. A significant reduction in head generation was observed for a single operating point compared to the previous study, giving better agreement with the referenced experimental data [31]. Performance map calculations conducted for three rotational speeds in [32] showed that the shares of fluid zones located close to the impeller leading edges with state conditions in the two-phase region increase for higher rotational speeds, whereas a reversed dependency was observed regarding the regions close to the trailing edges.

Baltadjiev et al. [6] introduced a time scale ratio relating liquid droplet formation time to the residence time of flow under subcritical conditions in order to quantify the possibility of condensation within a low-flow-coefficient sCO_2 compressor stage. For all investigated operating conditions away from the critical point, the time scale ratio was much smaller than one, suggesting improbability of condensation. Nevertheless, the authors pointed out that a time scale ratio of 1 could be reached for operating points that are more closely located to the critical point, due to an increased subcritical expansion and asymptotically vanishing surface tension.

3D RANS simulations of the SNL compressor were also conducted by Ameli et al. [1; 3], who focused on the effects of lookup table resolution of the applied bilinear interpolation routine on performance and flow field predictions. It was shown that higher table resolutions resulted in a better agreement with experimental data regarding efficiency, whereas the assessment of pressure ratio proved to be rather insensitive. Especially, the resolution of near-critical properties was stressed, as the authors stated that 0.5 % error in the lookup table can have a significant impact on the performance prediction at close-critical operating conditions. The authors also showed that higher table resolutions resulted in an increased assessment of flow regions within the two-phase region because of lower values of speed of sound.

In a preliminary study prior to this work [19], the performance as well as the flow field of an impeller geometry resembling the main dimensions of the SNL main compressor were investigated. Reasonable performance metrics were derived for two compressor inlet states lying in the supercritical and gas phase region, respectively. A high degree of machine similitude was observed for compressor operation at these inlet states through a non-dimensional performance curve representation. Similar to the observations from the authors referenced before, the flow field highlighted fluid zones inside the vapour-liquid region near the blade leading edge suction sides due to flow acceleration. These were quantified by their volumetric share for different flow coefficients. Contrary to previously cited authors, who all used bilinear interpolation techniques to account for the thermophysical properties of CO_2, property table interpolation was conducted through the Spline-Based-Table-Lookup Method (SBTL) [20; 21]. The method indicated low computational overhead compared to an ideal gas reference calculation while providing accuracies within the deviation of the underlying state equation, being the Span-Wagner equation of state [35].

Building on the previous work [19], this study extends the compressor performance testing to also account for the channel type diffuser that was not modeled before. This is believed to improve the comparability with the experimental results as a vaned

diffuser can generally reduce the operating range and also exhibit upstream effects. In order to provide a further reference for the previous and current performance assessments, a meanline analysis based on internal and external loss models, originally qualified for the application with conventional compressors, will be conducted. In this way, also the applicability of respective models for the application with regard to CO_2 compressors can be evaluated.

The paper is structured as follows. First, the numerical framework comprising the in-house CFD solver and the real gas tabulation approach as well as the meanline analysis procedure will be presented. Afterwards, a test case description will be provided followed by an description of the deduced compressor stage geometry and numerical setup. Results of the numerical analysis methods will be compared with each other and to data from the previous study [19] as well as experimental results reported by Wright et al. [38; 39] and Fuller & Eisemann [14].

3D CFD PROCEDURE

A density based compressible in-house CPU/GPU hybrid CFD solver [29] is applied for simulations in this work. The Navier-Stokes equations

$$\partial_t \underline{w} + \operatorname{div}\left(\underline{\underline{F}}^a - \underline{\underline{F}}^d\right) = \underline{s}, \tag{1}$$

complemented by constitutive equations as well as expressions for thermodynamic state are solved in their Reynolds-averaged form. Conservative variables, flux terms and source terms are specified as follows (given for the absolute frame of reference for brevity):

$$\underline{w} := (\rho, \rho\underline{u}, \rho E) \tag{2}$$

$$\underline{\underline{F}}^a := \left(\rho\underline{u}, \rho\underline{u}\otimes\underline{u} + p\underline{\underline{I}}, \rho\underline{u}H\right) \tag{3}$$

$$\underline{\underline{F}}^d := \left(\underline{0}, \underline{\underline{\tau}}, \underline{u}\cdot\underline{\underline{\tau}} - \underline{q}\right) \tag{4}$$

$$\underline{s} := \underline{0}. \tag{5}$$

The applied formulation of the NS-equations for the rotating frame of reference is given in [27]. The viscous shear stress tensor and the heat flux vector are defined through Stokes' and Fourier's law for a Newtonanian fluid, respectively:

$$\underline{\underline{\tau}} := \mu(\rho, e)\left(\operatorname{grad}\underline{u} + (\operatorname{grad}\underline{u})^T - 2/3\operatorname{div}\underline{u}\,\underline{\underline{I}}\right) \tag{6}$$

$$\underline{q} := -\lambda(\rho, e)\operatorname{grad}T(\rho, e). \tag{7}$$

Spatial discretisation is performed on structured grids applying a finite-volume approach. Advective fluxes are discretised based on a second order AUSM+ scheme [28] utilising a piecewise linear MUSCL reconstruction [36] and central scheme discretisation is applied for diffusive fluxes. The resulting ordinary differential equations are integrated in time through an implicit LUSGS scheme and the Spalart-Allmaras turbulence model [34] is employed for closure of the RANS equations. Recent solver applications comprise the thematic fields of non-equilibrium wet steam [29], including the first LES of a condensing wet steam cascade [30], humid air [16], and sCO_2 [19].

REAL GAS PROPERTY TABULATION

Thermophysical properties of CO_2 are derived from the Span-Wagner multiparameter reference equation of state (SW-EOS) as well correlations for molecular viscosity and thermal conductivity given by Laesecke et al. [22] and Huber et al. [15], respectively. As the SW-EOS is too computationally expensive in the context of a 3D CFD simulation, all thermophysical properties are pre-computed and accessible in the solver via a software library applying the Spline-Based Table Look-Up Method (SBTL) [20; 21]. The SBTL was developed for the fast calculation of thermophysical properties in complex process simulations. Based on spline interpolation techniques applying lower order polynomials, such as biquadratic or bicubic spline functions, the SBTL overcomes fundamental problems adherent to local interpolation routines, e.g. the most commonly applied bilinear interpolation method. Unlike local bilinear interpolation, biquadratic spline functions yield continuous first derivatives. Moreover, biquadratic spline polynomials can be solved quickly with regard to their independent variables. Hence, numerically consistent backwards functions can be calculated, which are faster than those obtained from the inversion of bicubic polynomials. Furthermore, simple search algorithms can be applied due to the construction of splines on piecewise equidistant nodes of transformed variables, allowing for linearisation.

Tabulation is performed based on density and internal energy as the independent thermodynamic variables of choice because these can be directly deduced from the conservative variables:

$$\rho(\underline{w}) = \rho, \;\; e(\underline{w}) = \rho^{-1}\left(\rho E - (2\rho)^{-1}\rho\underline{u}\right). \tag{8}$$

The range of validity of the SBTL property library is specified as follows: 216.59 K $\leq T \leq$ 1300 K; 0.5 kPa $\leq p \leq$ 100 MPa. Permissible deviations of SBTL spline functions are listed in table 1. These are within the uncertainties of the underlying EOS and transport property correlations, except at the critical point, where isobaric heat capacity and thermal conductivity become infinite.

In all simulations, thermodynamically stable states are considered only, i.e. fluid properties in the vapour-liquid region are calculated as a homogenous equilibrium mixture.

TABLE 1: Permissible deviations for the development of SBTL functions from the reference equation of state by Span and Wagner [35] as well as the correlations for viscosity and thermal conductivity [15; 22]

SBTL function		liquid region	gas region
$p(v,e)$	$p \leq 2.5$ MPa	$\lvert\Delta p/p\rvert < 10^{-5}$	$\lvert\Delta p/p\rvert < 10^{-5}$
	$p > 2.5$ MPa	$\lvert\Delta p\rvert < 0.5$ kPa	
$T(v,e)$		$\lvert\Delta T\rvert < 1$ mK	$\lvert\Delta T\rvert < 1$ mK
$s(v,e)$		$\lvert\Delta s\rvert < 10^{-6}\,\frac{\text{kJ}}{\text{kgK}}$	$\lvert\Delta s\rvert < 10^{-6}\,\frac{\text{kJ}}{\text{kgK}}$
$a(v,e)$		$\lvert\Delta a/a\rvert < 10^{-5}$	$\lvert\Delta a/a\rvert < 10^{-5}$
$\lambda(v,e)$[1]		$\lvert\Delta\lambda/\lambda\rvert < 10^{-5}$	$\lvert\Delta\lambda/\lambda\rvert < 10^{-5}$
$\mu(v,e)$		$\lvert\Delta\mu/\mu\rvert < 10^{-5}$	$\lvert\Delta\mu/\mu\rvert < 10^{-5}$

[1] The correlation of the thermal conductivity [15] shows some discontinuities along the $T = 1.5 \cdot T_c = 456.1923$ K isotherm. Along this isotherm, the deviations in thermal conductivity are larger than the permissible values but within the uncertainty of the underlying correlation itself.

MEANLINE ANALYSIS PROCEDURE

The meanline analysis is performed sequentially as well as iteratively for the stage components and applies a single-zone modelling approach. A loss model set proposed and validated by Oh et al. [25] for the application with centrifugal compressors operating with conventional working fluids obeying the ideal gas law is incorporated in the impeller analysis. Recently, the loss model set was also utilised for performance calculations of sCO_2 compressors by different researchers and stated to be applicable [2; 23; 33]. The set was suggested on basis of various possible combinations of most of the internal and external loss models in the literature. It accounts for six mechanisms of internal and three sources of external (parasitic) losses, the latter giving rise to the impeller stagnation enthalpy without contributing to pressure rise:

$$\Delta h_t = W_{Euler} + \sum W_{external} \quad \text{(assuming adiabatic flow)}. \tag{9}$$

An overview of the applied loss correlations, which are formulated as enthalpy losses, is presented in table A1 for the reader's convenience. Also, a schematic h,s-diagram is presented in figure 1 illustrating the impeller process path and the contribution of internal and external losses. Complementary to the loss models, the common slip correlation

$$\sigma = 1 - \frac{\sqrt{\cos\beta_{2,bl}}}{Z_{bl}^{0.7}} \quad \text{(meridional angle system)}, \tag{10}$$

based on the formulation by Wiesner [37] is applied in order to assess the actual work input and deviation angle compared to the idealised case where the fluid would be perfectly guided by the impeller blades:

$$W_{Euler} = u_2 c_{2\theta} - u_1 c_{1\theta} = u_2\left(\sigma u_2 + c_{2m}\tan\beta_{2,bl}\right). \tag{11}$$

The applied vaned diffuser analysis is based on a modelling approach presented by Aungier [5]. Three sources of aerodynamic losses are adopted which are given in a total pressure loss coefficient formulation

$$p_{t4} = p_{t3} - (p_{t3} - p_3)\sum_i \bar{\omega}_i, \tag{12}$$

and are listed in table A1. The vaned diffuser discharge flow angle is computed by applying axial-flow compressor correlations transformed to the radial plane. Details are given in [5].

Within the meanline analysis, real gas thermophysical properties of CO_2 are considered through direct calls to the CoolProp property library [7].

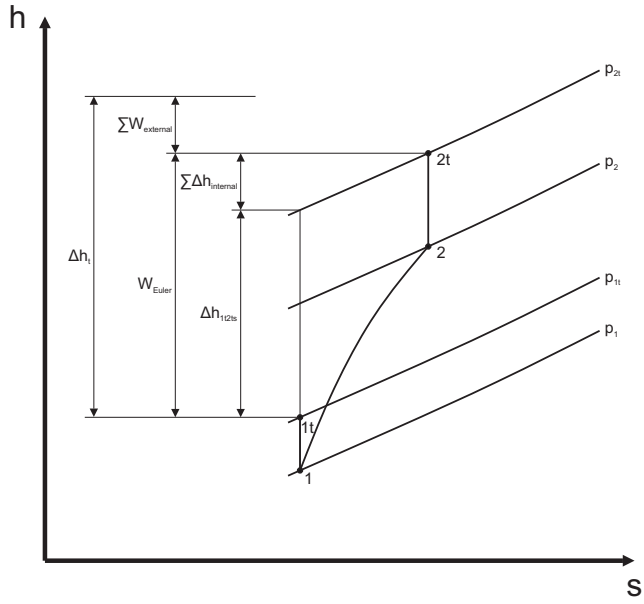

FIGURE 1: Schematic h,s-diagram illustrating the impeller process path as well as internal impeller loss and external loss contributions

sCO_2 COMPRESSOR TEST CASE

The main compressor installed in a sCO_2 compression test-loop which is operated by Sandia National Laboratories [39] is taken as a reference case. As only main dimensions of the

compressor are reported, this work investigates a newly generated compressor geometry resembling the same main dimensions. The SNL main compressor stage comprises a backward swept impeller with splitter blades and a channel type (wedge) diffuser. It is designed for operation at a total inlet state that thermodynamically lies close to the critical point of carbon dioxide ($T_t/T_c \approx 1.004, p_t/p_c \approx 1.042$). The design rotational speed is specified with 75 krpm and the design mass flow rate is given as 3.5 kg/s. Expressed through non-dimensional parameters, the given specifications correspond with a flow coefficient of $\phi = 0.037$ and a peripheral Mach number of $Ma_u = 0.73$. The SNL compressor was designed by Barber Nichols Inc. on basis of a surrogate fluid that results in comparable key parameters based on turbomachinery similarity principles and which can be more closely approximated by an ideal gas model. It is stated that this approach provides a way to use existing loss models and design tools [39].

The SNL main compressor has undergone extensive experimental investigations [14; 38; 39], most notably performance tests. Because a comparison of numerical results with experimental performance data is subject to this work, knowledge of the experimental instrumentation and data assessment is important to ensure comparability with regard to an appropriate numerical setup and postprocessing of data. Resistance temperature detectors and total pressure transducers were installed at the stage inlet and outlet. In addition, a static pressure tap was located at the impeller exit [38; 39]. Hence, reported experimental total-to-static performance data is interpreted to refer to the impeller. Accordingly, it is stated that isentropic impeller efficiencies were assessed through meanline analysis codes and compared to experimental data [38]. Although it is principally possible to deduce enthalpy and ultimately efficiency from temperature and pressure measurements in the supercritical state, it is important to note that enthalpy is extremely sensitive to small changes of these state variables. As a matter of fact, experimental efficiencies were derived from electrical power measurements with corrections for electric and mechanical losses rather than enthalpy calculations from measured pressures and temperatures [38]. Note, that the exact positions of the measuring devices were not reported.

TABLE 2: Compressor stage main dimensions taken from [39]

Number of impeller main / splitter blades	6 / 6	
Inducer shroud radius	9.37	[mm]
Inducer hub radius	2.54	[mm]
Inducer blade angle at tip	50	[deg]
Impeller exit radius	18.68	[mm]
Impeller exit width	1.71	[mm]
Impeller exit blade angle (backswept)	-50	[deg]
Impeller blade thickness	0.76	[mm]
Number of diffuser blades	17	
Diffuser exit vane angle	71.5	[deg]

GEOMETRY GENERATION AND COMPUTATIONAL SETUP

In a preliminary study [19], only the impeller wheel of SNL main compressor was considered. In this work, the investigated geometry is extended to account for the full compressor stage comprising a channel type diffuser. No detailed blade coordinates are publicly reported for the reference case and only partial information on main dimensions is given in [39]. Thus, a compressor geometry with similar main dimensions is designed and investigated in this work. All publicly reported main dimensions are listed in table 2 for the reader's convenience. Additional geometric data was deduced from part drawings depicted in [14; 39] and the final compressor design (see figure 3) was generated through a preliminary compressor design/analysis tool and its interface to a 3D blade generation module [9; 10].

The computational domain was created with an automated multi-block structured mesh generator [24] and is reduced to the consideration of a single impeller and diffuser passage due to rotational periodicity and the applied mixing-plane rotor-stator interface approach. Within each blade row, full one-to-one grid connections avoid the need for interpolation between adjacent blocks. The mesh size counts approximately 1.5 million cells for the impeller and 630.000 cells for the diffuser passage. While free-stream and inter-blade regions are meshed through H-grid topologies, O-grid topologies are applied at near-blade areas. The computational grid is shown in figure 2.

Total pressure and total temperature as well as a uniform normal direction of flow along with a turbulent viscosity ratio are specified as boundary conditions at the domain inlet. A constant static pressure is defined at the outlet of the vaneless space prolongation. All walls are treated as adiabatic and the no-slip condition is applied.

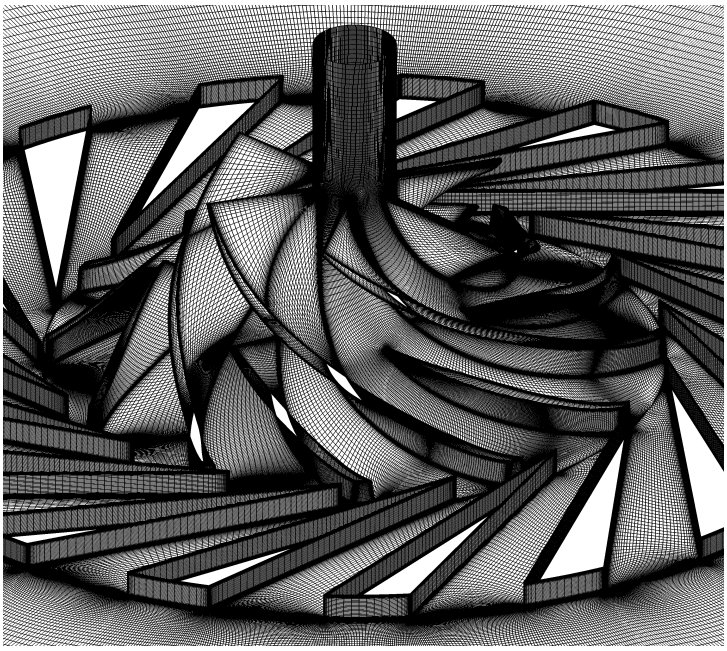

(a)

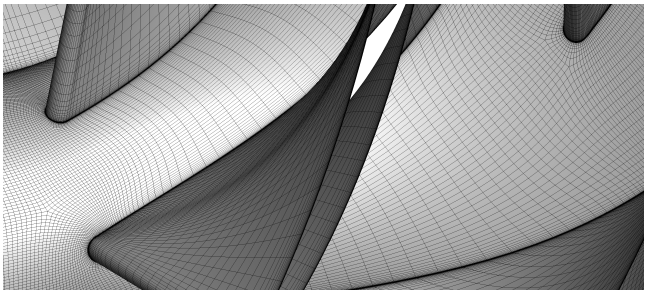

(b)

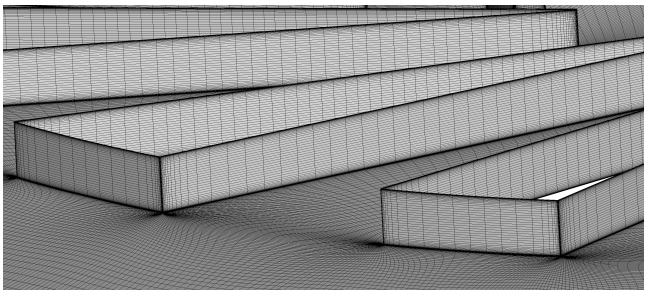

(c)

FIGURE 2: Computational grid (repeated surface representation): (a) Stage view, (b) Impeller main and splitter blade leading edge region, (c) Channel diffuser trailing edge region

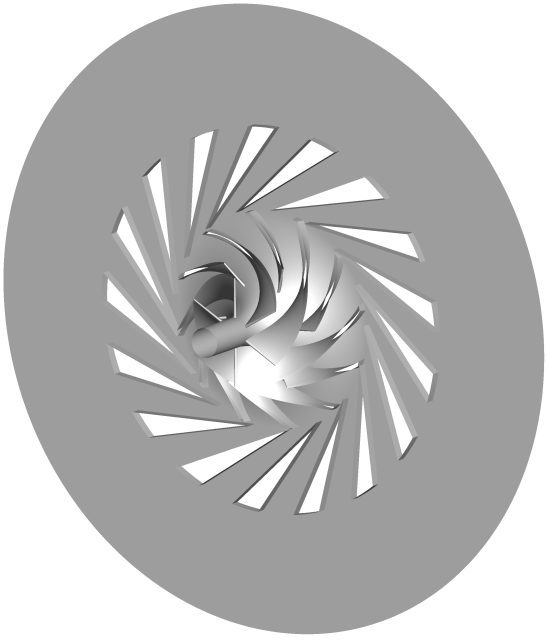

FIGURE 3: 3D model of the compressor stage based on main dimensions of the SNL main compressor

PERFORMANCE ANALYSIS

In a previous study [19], the performance characteristics of the impeller wheel were numerically assessed for two distinct inlet states - a close-critical operating state near the design condition and a subcritical compressor inlet state in the gas phase, the latter being potentially relevant during cycle startups [14]. For both investigated states, almost identical non-dimensional performance curves were derived, indicating a high degree of machine similarity and thus, high relaxation of the dependency on the inlet state by applying a non-dimensional representation. In this work, the performance testing is extended to account for a configuration including a channel type diffuser and is conducted at a supercritical compressor total inlet condition at $T_t/T_c \approx 1.03$ and $p_t/p_c \approx 1.05$. The candidate state point is depicted in the T,s-diagram in figure 4, together with an underlaid contour line plot of the compressibility factor

$$Z = p/(\rho RT), \tag{13}$$

indicating the highly non-ideal thermodynamics of the operating regime.

The performance assessment is conducted at 50 krpm rotational speed as most of the experimental data provided by Wright et al. [38; 39] and exclusively all of the data given by Fuller & Eisemann [14] for the SNL reference case were obtained at this rotational speed. Note, that no experimental data is reported for the design rotational speed at 75 krpm and no ef-

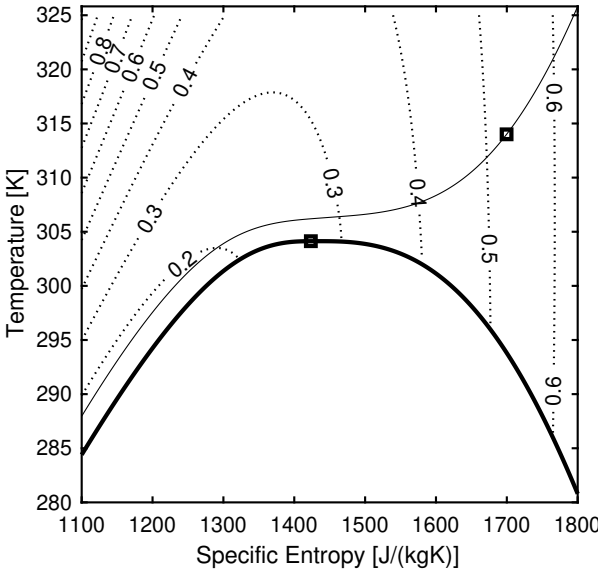

FIGURE 4: T,s-diagram showing the investigated compressor total inlet state at $T_t = 314$ K, $p_t = 77.5$ bar. Contour lines illustrate the compressibility factor.

ficiency data is provided by Fuller & Eisemann [14]. Because of extreme deviations in the experimental inlet states, e.g. accounting for variations of total density in the range $(344...686) kg/m^3$ for the data set specified by Wright et al. [39], all reference data is provided in either corrected or non-dimensional form. The same set of non-dimensional performance parameters, as applied in the preceeding study [19], is adopted here for the sake of comparison: The ideal head coefficient

$$\psi = \left(h_{i,s} - h_{1,t}\right) / u_2^2 \tag{14}$$

and the total-to-static isentropic efficiency

$$\eta_s = \left(h_{i,s} - h_{1,t}\right) / \left(h_{2,t} - h_{1,t}\right), \tag{15}$$

are both illustrated as a function of the flow coefficient

$$\phi = 4 \cdot \dot{V}_1 / \left(\pi \cdot d_2^2 \cdot u_2\right). \tag{16}$$

Note, that the index i in equation 14 and equation 15 refers either to the intrastage (between the impeller trailing edge and the channel diffuser leading edge) or the stage exit position evaluated at $r/r_2 = 1.008$ and $r/r_2 = 2.055$, respectively.

Figure 5 shows the non-dimensional performance curve representation of the conducted RANS and meanline calculations, which are both evaluated at the intrastage and stage exit position. Additionally, the experimental data reported by Wright et al. [38; 39] and Fuller & Eisemann [14] as well as results of the previous RANS study [19] analysing the sole impeller geometry (followed by some vaneless space) are presented. As the meanline analysis is applied sequentially, an evaluation at the intrastage position is analogous to the sole consideration of the

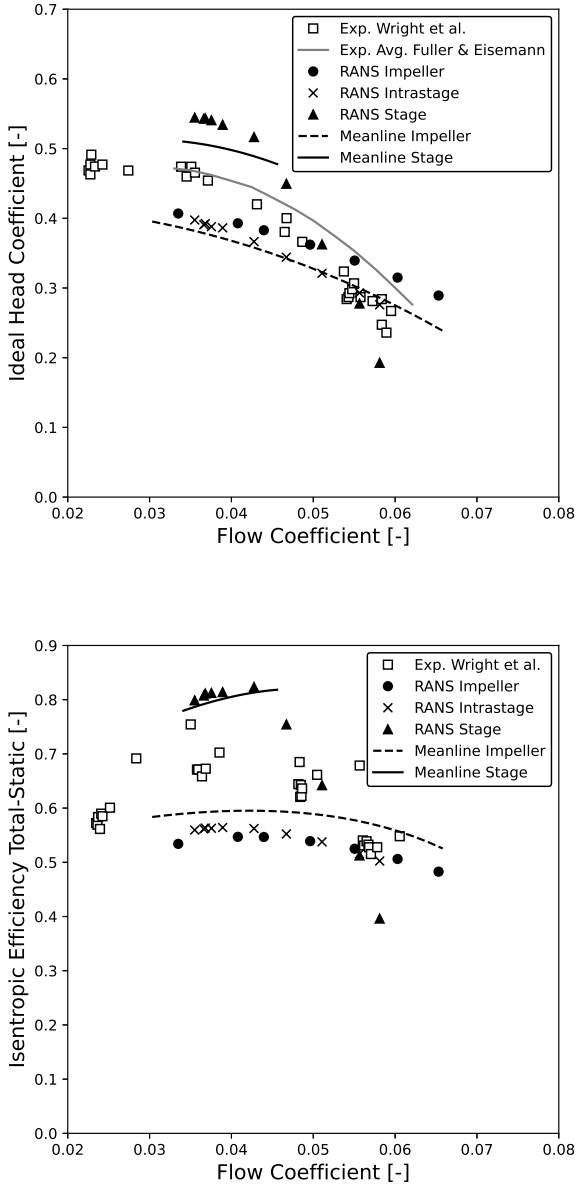

FIGURE 5: Non-dimensional compressor performance. Experimental data refer to Wright et al. [38; 39][1] and Fuller & Eisemann [14]. The latter did not report efficiency data. RANS simulations of the standalone impeller geometry were conducted in [19].

impeller.

Comparing both RANS calculations evaluated behind the impeller exit, a steeper ideal head characteristic is obtained through a performance assessment of the channel diffuser stage

configuration. This difference might be attributed to the short radial distance between the impeller trailing and diffuser leading edges (measuring merely 0.3 mm) and associated increase of static pressure due to close locations of stagnation points near the evaluation plane. Both ideal head curves are noticeably flatter compared to those of the experimental data sets, which might be owed to geometric disparities between the real compressor geometry and the investigated design based on similar main dimensions. In particular, deviations in blade angle distributions might affect head generation. Also, differences in the uncertain data assessment positions could lead to discrepancies, especially regarding static flow quantities. However, the impeller meanline analysis, also conducted on basis of main dimensions, is in much better agreement with the CFD data regarding the slope of the impeller ideal head characteristic. This observation is important to note because it shows that both numerical methodologies, which share the same input of data, also show consistent trends in their output. In particular, good agreement between the impeller meanline analysis and the intrastage RANS evaluation can be observed, indicating the applicability of the associated impeller aerodynamic loss models for compressors operating with sCO_2.

With regard to calculated impeller isentropic efficiencies, no significant quantitative discrepancies can be observed between the two RANS assessments, which show about ten percentage points reduced maximum efficiencies compared to the experimental data exhibiting a high degree of scatter by outliers. Note, that experimental efficiencies were derived from motor power measurements and corrections for mechanical and electric losses through correlations, which also entain uncertainties. Because of the exclusion of external losses in the experiments, external losses are also excluded within this meanline study. This also ensures better comparability with the conducted RANS simulations, where these are not assessed. A good agreement with the experimental flow coefficient value at which the maximum impeller efficiency is obtained is noticed for the RANS calculation evaluated at the intrastage plane. Respective values are in accordance with the design flow coefficient of the machine stated earlier. The meanline isentropic impeller efficiency characteristic agrees well with CFD data with regard to its shape, but shows slightly higher values over the entire flow range and a maximum efficiency of about 60 %. This can be expected, as only a limited number of loss contributing mechanisms is assessed through the meanline approach.

An ideal head rise of 13-41 % is observed in the flow range of $\phi \approx 0.036...0.051$ by considering the channel type diffuser in the RANS simulations conducted in this study. For higher flow coefficients, the diffuser increasingly fails to provide recovery of ideal head. The meanline analysis comprising the diffuser shows about 6-7 % reduced ideal head compared to the RANS calculations for flow coefficients up to $\phi \approx 0.043$ and demonstrates a good agreement regarding efficiency for this flow range. However, for higher flow coefficients, the applied diffuser model formulation is not able to resemble the abrupt decline in ideal stage head as well as isentropic efficiency, as indicated by the CFD analysis. The fact that a rapid decrease of the ideal head or isentropic efficiency characteristic can not be observed in the provided experimental data indicates that the interpretation of these data sets being associated with the impeller wheel holds plausible and likely.

CONCLUSION AND OUTLOOK

In this work, the performance characteristics of a centrifugal compressor stage operating with supercritical CO_2 are investigated by means of 3D RANS simulations as well as a single-zone meanline analysis procedure applying loss correlations. In order to account for thermophysical real gas properties, the applied in-house density based compressible CFD solver is coupled to a software library implementation of the Spline-based Table Look-Up Method (SBTL) [20; 21] adopted for CO_2 applications. The investigated compressor stage is based on main dimensions of a test-loop compressor operated by Sandia National Laboratories. The compressor performance is assessed for a supercritical inlet operation state through a non-dimensional speed curve representation, which is compared to experimental data as well as numerical data obtained from a preceeding study [19], in which only the impeller geometry was considered.

With regard to the previous study, a steeper impeller head curve is derived through the CFD analysis considering the complete stage geometry. This indicates a noticeable upstream effect of the channel diffuser located closely to the impeller trailing edge. However, impeller efficiencies previously derived on basis of the simplified geometry considering a standalone impeller are comparable in quality as well as quantity. The overall trends regarding the impeller performance are satisfyingly resembled by the meanline analysis, which suggests the applicability of the applied internal loss model set and slip correlation for performance predictions of sCO_2 impellers.

A potential ideal head rise of up to 41 % through the channel type diffuser is identified by the RANS calculations. However, this potential diminishes abruptly for flow coefficients exceeding values of $\phi \approx 0.043$. This behaviour can not be resembled by the applied diffuser model in the meanline approach. Nevertheless, the meanline analysis provides a good agreement with CFD data in the flow coefficient range where practical recovery of ideal head is predicted, thus, also suggesting applicability of respective conventional diffuser loss and deviation models for CO_2 compressors, provided that real gas properties are accounted for in the general meanline procedure.

Transient simulations of the compressor will be subject to future research in order to increase the fidelity of the performance assessment considering dynamic rotor-stator-interaction.

NOMENCLATURE

Abbreviations

Avg.	average
CFD	computational fluid dynamics
EOS	equation of state
Exp.	experiment
RANS	Reynolds-Averaged Navier Stokes
SBTL	Spline-Based Table Look-Up Method
sCO_2	supercritical carbon dioxide
SNL	Sandia National Laboratories
SW	Span-Wagner

Subscripts

1	impeller inlet
2	impeller exit
3	channel diffuser inlet
4	channel diffuser exit
bl	blading
c	critical
i	station index
s	isentropic
t	total

Symbols

$\bar{\omega}$	total pressure loss coefficient
β	relative flow angle
$\dot{V}$	volume flow
η_s	total-to-static isentropic efficiency
λ	thermal conductivity coefficient
μ	dynamic viscosity
ϕ	flow coefficient
ψ	ideal head coefficient
ρ	density
σ	slip factor
$\underline{\underline{\tau}}$	stress tensor
$\underline{\underline{F}}^a$	advective flux tensor
$\underline{\underline{F}}^d$	diffusive flux tensor
$\underline{\underline{I}}$	identity tensor
$\underline{q}$	heat flux vector
$\underline{s}$	source term vector
$\underline{u}$	velocity vector
$\underline{w}$	conservative variables vector
a	speed of sound
d_2	impeller tip diameter
E	specific total internal energy
e	specific internal energy
H	specific total enthalpy
h	specific enthalpy
Ma_u	peripheral Mach number
p	pressure
R	specific gas constant
T	temperature
t	time variable
u_2	impeller tip speed
W	specific work
Z	compressibility factor
Z_{bl}	number of blades

References

[1] Ameli, A., Turunen-Saaresti, T., and Backman, J. (2016). Numerical Investigation of the Flow Behavior Inside a Supercritical CO_2 Centrifugal Compressor. *Proceedings of the ASME Turbo Expo 2016*. ASME Paper No. GT2016-57481.

[2] Ameli, A. et al. (2018a). Compressor Design Method in the Supercritical CO_2 Applications. *Supercritical CO_2 Power Cycles Symposium 2018*. Pittsburgh, Pennsylvania, USA.

[3] Ameli, A. et al. (2018b). Effects of Real Gas Model Accuracy and Operating Conditions on Supercritical CO_2 Compressor and Flow Field. *Journal of Engineering for Gas Turbines and Power*, 140(6).

[4] Aungier, R. H. (1995). Mean Streamline Aerodynamic Performance Analysis of Centrifugal Compressors. *Journal of Turbomachinery*, 117(3):360–366.

[5] Aungier, R. H. (2000). *Centrifugal Compressors. A Strategy for Aerodynamic Design and Performance Analysis*. ASME Press.

[6] Baltadjiev, N. D., Lettieri, C., and Spakovszky, Z. S. (2015). An Investigation of Real Gas Effects in Supercritical CO_2 Compressors. *Journal of Turbomachinery*, 137(9).

[7] Bell, I. et al. (2014). Pure and Pseudo-pure Fluid Thermophysical Property Evaluation and the Open-Source Thermophysical Property Library CoolProp. *Industrial & Engineering Chemistry Research*, 53(6):2498–2508.

[8] Brun, K., Friedman, P., and Dennis, R. (2017). *Fundamentals and Applications of Supercritical Carbon Dioxide (sCO_2) Based Power Cycles*. Woodhead Publishing.

[9] Concepts NREC LLC (2018a). AxCent64 (8.7.13.0).

[10] Concepts NREC LLC (2018b). Compal (8.7.13.0).

[11] Conrad, O., Raif, K., and Wessels, M. (1979). The Calculation of Performance Maps for Centrifugal Compressors With Vane-Island Diffusers. *Proceedings of the Twenty-fifth Annual International Gas Turbine Conference and Exhibit and Twenty-second Annual Fluids Engineering Conference*. New Orleans, Louisiana, USA.

[12] Coppage, J. E. et al. (1956). Study of Supersonic Radial Compressors for Refrigeration and Pressurization Systems. WADC TECHNICAL REPORT 55-257, Airesearch Manufacturing Company.

[13] Daily, J. W. and Nece, R. E. (1960). Chamber Dimension Effects on Induced Flow and Frictional Resistance of Enclosed Rotating Disks. *Journal of Basic Engineering*, 82(1):217–230.

[14] Fuller, R. L. and Eisemann, K. (2011). Centrifugal Compressor Off-Design Performance for Super-Critical CO_2. *Super-*

critical CO_2 Power Cycles Symposium 2011. Boulder, Colorado, USA.

[15] Huber, L. and Sykioti, E. A. (2016). Reference Correlation of the Thermal Conductivity of Carbon Dioxide from the Triple Point to 1100 K and up to 200 MPa. *Journal of Physical and Chemical Reference Data*, 45(1).

[16] Iseni, S., Post, P., and di Mare, F. (2019). Numerical Analysis of the Influence of Air Humidity on a Transonic Compressor Stage. *International Gas Turbine Congress 2019*. Paper No. ThAM16.1, Tokyo.

[17] Jansen, W. (1967). A Method for Calculating the Flow in a Centrifugal Impeller When Entropy Gradients Are Present. *Royal Society Conference on Internal Aerodynamics (Turbomachinery)*. Cambridge, UK.

[18] Johnston, J. P. and Dean, R. C., Jr. (1966). Losses in Vaneless Diffusers of Centrifugal Compressors and Pumps: Analysis, Experiment, and Design. *Journal of Engineering for Power*, 88(1):49–60.

[19] Karaefe, R. E. et al. (2020). Numerical Investigation of a Centrifugal Compressor for Supercritical CO_2 Cycles. *Proceedings of the ASME Turbo Expo 2020*. ASME Paper No. GT2020-15194, 2020.

[20] Kunick, M. (2018). Fast Calculation of Thermophysical Properties in Extensive Process Simulations with the Spline-Based Table Look-Up Method (SBTL). *Fortschrittberichte VDI*. Nr. 618, Reihe 6, Energietechnik.

[21] Kunick, M. et al. (2015). CFD Analysis of Steam Turbines With the IAPWS Standard on the Spline-Based Table Look-Up Method (SBTL) for The Fast Calculation of Real Fluid Properties. *Proceedings of the ASME Turbo Expo 2015*. ASME Paper No. GT2015-43984.

[22] Laesecke, A. and Muzny, C. D. (2017). Reference Correlation for the Viscosity of Carbon Dioxide. *Journal of Physical and Chemical Reference Data*, 46(1).

[23] Lee, J. et al. (2012). Design Methodology of Supercritical CO_2 Brayton Cycle Turbomachineries. *Proceedings of the ASME Turbo Expo 2012*. ASME Paper No. GT2012-68933.

[24] NUMECA International (2018). AutoGrid5 (13.1).

[25] Oh, H. W., Yoon, E. S., and Chung, M. K. (1997). An Optimum Set of Loss Models for Performance Prediction of Centrifugal Compressors. *Proceedings of the Institution of Mechanical Engineers, Part A: Journal of Power and Energy*, 211(4):331–338.

[26] Pecnik, R., Rinaldi, E., and Colonna, P. (2012). Computational Fluid Dynamics of a Radial Compressor Operating with Supercritical CO_2. *Journal of Engineering for Gas Turbines and Power*, 134(12).

[27] Post, P. (2020). *Development of Efficient Numerical Methods for Non-Ideal Compressible Fluid Flows in Propulsion and Power*. PhD thesis, Ruhr-Universität Bochum.

[28] Post, P. and di Mare, F. (2018). Highly Efficient Euler-Euler Approach for Condensing Steam Flows in Turbomachines. *GPPS 2018*. Montreal, Canada.

[29] Post, P., Sembritzky, M., and di Mare, F. (2019). Towards Scale Resolving Computations of Condensing Wet Steam Flows. *Proceedings of the ASME Turbo Expo 2019*. ASME Paper No. GT2019-91269.

[30] Post, P., Winhart, B., and di Mare, F. (2020). Large Eddy Simulation of a Condensing Wet Steam Turbine Cascade. *Proceedings of the ASME Turbo Expo 2020*. ASME Paper No. GT2020-16064, 2020.

[31] Rinaldi, E., Pecnik, R., and Colonna, P. (2013). Steady State CFD Investigation of a Radial Compressor Operating with Supercritical CO_2. *Proceedings of the ASME Turbo Expo 2013*. ASME Paper No. GT2013-94580.

[32] Rinaldi, E., Pecnik, R., and Colonna, P. (2015). Computational Fluid Dynamic Simulation of a Supercritical CO_2 Compressor Performance Map. *Journal of Engineering for Gas Turbines and Power.*, 137(7).

[33] Romei, A. et al. (2020). The Role of Turbomachinery Performance in the Optimization of Supercritical Carbon Dioxide Power Systems. *Journal of Turbomachinery*, 142(7).

[34] Spalart, P. R. and Allmaras, S. R. (1992). A One-Equation Turbulence Model for Aerodynamic Flows. *30th Aerospace Sciences Meeting and Exhibit*.

[35] Span, R. and Wagner, W. (1996). A New Equation of State for Carbon Dioxide Covering the Fluid Region from the Triple-Point Temperature to 1100 K at Pressures up to 800 MPa. *Journal of Physical and Chemical Reference Data*, 25(6):1509–1596.

[36] van Leer, B. (1979). Towards the Ultimate Conservative Difference Scheme. V. A Second-Order Sequel to Godunov's Method. *Journal of Computational Physics*, 32(1).

[37] Wiesner, F. J. (1967). A Review of Slip Factors for Centrifugal Impellers. *Journal of Engineering for Gas Turbines and Power*, 89(4):558–566.

[38] Wright, S. A. et al. (2009). Supercritical CO_2 Compression Loop Operation and Test Results. *Supercritical CO_2 Power Cycles Symposium*. Troy, NY, USA.

[39] Wright, S. A. et al. (2010). Operation and Analysis of a Supercritical CO_2 Brayton Cycle. SANDIA REPORT SAND2010-0171, Sandia National Laboratories.

Annex A

TABLE A1: Set of internal and external (parasitic) loss models

Loss mechanism	Loss model		Reference
Impeller:			
Incidence	$\Delta h_{inc} = \sigma \cdot \frac{\left(w_{1\theta} - w_{1\theta,bl}\right)^2}{2}$	$\sigma = 0.5...0.7$	Conrad et al. [11]
Blade loading	$\Delta h_{bl} = 0.05 \cdot D_f^2 \cdot u_2^2$	$D_f = 1 - \frac{w_2}{w_{1t}} + \frac{0.75 \cdot W_{Euler}/u_2^2}{w_{1t}/u_2 \left[\frac{Z_{bl}}{\pi}\left(1 - \frac{d_{1t}}{d_2}\right) + 2\frac{d_{1t}}{d_2}\right]}$	Coppage et al. [12]
Skin friction	$\Delta h_{sf} = 2 c_f \frac{L_{fl}}{d_{hb}} \bar{w}^2$	$\bar{w} = \frac{\left(2w_2 + w_{1t} - w_{1h}\right)}{4}$	Jansen [17]
		$L_{fl} \approx \frac{\pi}{8}\left(d_2 - \frac{d_{1t}+d_{1n}}{2} - b_2 + 2L_{ax}\right)\left(\frac{2}{\frac{\cos\beta_{1t}+\cos\beta_{1h}}{2} + \cos\beta_2}\right)$	
		$d_{hb} = \frac{d_2 \cos\beta_2}{\frac{Z_{bl}}{\pi} + \frac{d_2 \cos\beta_2}{b_2}} + \frac{\frac{d_2}{2}\left(\frac{d_{1t}}{d_2} + \frac{d_{1h}}{d_2}\right)\left(\frac{\cos\beta_{1t}+\cos\beta_{1h}}{2}\right)}{\frac{Z_{bl}}{\pi} + \left(\frac{d_{1t}+d_{1n}}{d_{1t}-d_{1n}}\right)\left(\frac{\cos\beta_{1t}+\cos\beta_{1h}}{2}\right)}$	
		$c_f = 0.0412 Re^{-0.1925}; Re = \frac{d_{hb}\bar{w}}{\nu}$	
Clearance	$\Delta h_{cl} = u_2^2 0.6 \frac{\delta_{cl}}{b_2}\frac{c_{2\theta}}{u_2} \times \sqrt{\frac{4\pi}{b_2 Z_{bl}}\left[\frac{r_{1t}^2 - r_{1h}^2}{(r_2 - r_{1t})(1+\rho_2/\rho_1)}\right]}\frac{c_{2\theta}}{u_2}\frac{c_{1m}}{u_2}$		Jansen [17]
Mixing	$\Delta h_{mix} = \frac{c_2^2}{2\left[1+\left(c_{2\theta}/c_{2m}\right)^2\right]} \cdot \left[\frac{1-\varepsilon-B}{1-\varepsilon}\right]^2$		Johnston & Dean [18]
External:			
Disk friction	$W_{df} = f_{df}\frac{\bar{\rho} r_2^2 u_2^3}{4\dot{m}}$	$\bar{\rho} = \frac{\rho_1+\rho_2}{2}$; $f_{df} = \begin{cases} \frac{2.67}{Re_{df}^{0.5}}, & Re_{df} < 3\cdot 10^5 \\ \frac{0.0622}{Re_{df}^{0.2}}, & Re_{df} \geq 3\cdot 10^5 \end{cases}$	Daily & Nece [13], as quoted by Oh et al. [25]
Recirculation	$W_{rc} = 8 \cdot 10^{-5} \sinh\left(3.5\alpha_2^3\right) D_f^2 u_2^2$		Oh et al. [25]
Leakage	$W_{lk} = \frac{\dot{m}_{cl} u_{cl} u_2}{2\dot{m}}$	$u_{cl} = 0.816\sqrt{2\Delta p_{cl}/\rho_2}$; $\dot{m}_{cl} = \rho_2 Z_{bl}\delta_{cl} L_{fl} u_{cl}$	Aungier [4]
		$\Delta p_{cl} = \frac{\dot{m}\left(r_2 c_{2\theta} - r_1 c_{1\theta}\right)}{Z_{bl}\bar{r}\bar{b}L_{fl}}$; $\bar{r} = \frac{r_1+r_2}{2}$; $\bar{b} = \frac{b_1+b_2}{2}$	
Channel Diffuser:			
Incidence	$\bar{\omega}_{inc} = \begin{cases} 0.8\left[\left(c_3 - c_3^*\right)/c_3\right]^2, & c_3 \leq c_{3S} \\ 0.8\left[\left(\left(c_3/c_{3S}\right)^2 - 1\right)c_{th}^2/c_3^2 + \left(c_{3S} - c_3^*\right)^2/c_{3S}^2\right], & c_3 > c_{3S} \end{cases}$		Aungier [5]
Skin friction	$\bar{\omega}_{sf} = 4 c_{f,diff}\left(\bar{c}/c_3\right)^2 L_B/d_{h,diff}/\left(2\delta/d_{h,diff}\right)^{0.25}$		Aungier [5]
Mixing	$\bar{\omega}_{mix} = \left[\left(c_{m,wake} - c_{m,mix}\right)/c_3\right]^2$		Aungier [5]

Note: Equations are presented for the meridional angle convention. The table nomenclature is given in SI-Units. B: ratio of diffuser inlet depth to impeller tip flow passage depth, b: width, c: absolute velocity, $c_{f,diff}$: diffuser skin friction coefficient, d: diameter, $d_{h,diff}$: average diffuser hydraulic diameter, h: specific enthalpy, L_{ax}: axial length of impeller, L_B: length of blade mean camberline, $\dot{m}$: mass flow, r: radius, u: peripheral velocity, W: specific work, w: relative velocity, Z_{bl}: number of blades, α: absolute flow angle, β: relative flow angle, δ_{cl}: clearance gap width, ε: fraction of blade-to-blade space occupied by the wake, μ: dynamic viscosity, ν: kinematic viscosity, ρ: density, $(\circ)_1$: impeller inlet, $(\circ)_2$: impeller exit, $(\circ)_3$: channel diffuser inlet, $(\circ)_{bl}$: blading, $(\circ)_h$: hub, $(\circ)_m$: meridional, $(\circ)_S$: value at onset of blade stall, $(\circ)_t$: tip, $(\circ)_{th}$: throat parameter, $(\circ)_\theta$: tangential, $(\circ)^*$: condition at minimum loss incidence angle

DOI: 10.17185/duepublico/73966
URN: urn:nbn:de:hbz:464-20210330-112107-5